The 2p absorption spectra of 3d transition metal compounds in tetrahedral and octahedral symmetry

1992 J. Phys.: Condens. Matter 4 4189

(http://iopscience.iop.org/0953-8984/4/16/019)

J. Phys.: Condens. Matter 4 (1992) 4189–4204. Printed in the UK

The 2p absorption spectra of 3d transition metal compounds in tetrahedral and octahedral symmetry

G van der Laan and I W Kirkman
SERC Daresbury Laboratory, Warrington WA4 4AD, UK

Received 3 January 1992

Abstract. We present the 2p ($L_{2,3}$) absorption spectra of first-row transition metal ions in tetrahedral and octahedral crystal field symmetry. These have been calculated using a localized description for the $3d^n$ to $2p^5 3d^{n+1}$ excitation including electrostatic and spin–orbit interactions. The spectra are significantly different from those already presented where the 3d spin–orbit interaction was neglected. The spectral shape provides a valence- and symmetry-selective probe. Whereas it changes gradually with the crystal field, abrupt changes in the spectra are indicative of high-spin to low-spin transitions. These spin transitions are accompanied by a strong decrease in the 2p branching ratio. The calculated spectra provide a basis for the use of $L_{2,3}$ absorption spectroscopy in materials science and biological science. The limitations of these calculations and the use of configuration interaction are discussed.

1. Introduction

It is well known that the K absorption edges of 3d transition metal compounds display an extended x-ray absorption fine structure (EXAFS) due to the scattering of the excited electron by the potential field of the neighbouring atoms. This effect can be used to determine bond distances and ligand coordination numbers. The information contained in the $L_{2,3}$ edges is of a completely different nature. The absorption spectrum is dominated by dipole transitions from the core 2p level to the empty 3d states, and because of the large Coulomb interaction between these two levels, it depends on the local electronic structure. Thus, analysis of the $L_{2,3}$ absorption structure may provide information about the oxidation state and the symmetry of the 3d transition metal ions. Further advantages are that the $2p_{3/2}$ and $2p_{1/2}$ spectral parts are clearly separated by the core–hole spin–orbit interaction, and that the core–hole lifetime broadening is small, resulting in sharp multiplet structures. The $L_{2,3}$ edges have not been studied as much as the K edge, because the energy region between 400 and 1000 eV was difficult to cover both with the grating and double-crystal monochromators. However, this situation has drastically changed in the last few years. A new generation of spherical grating monochromators offers a strongly improved energy resolution in this region [1], and the potential application of the $L_{2,3}$ edges has been demonstrated [2].

The 2p spectra cannot be described in terms of a one-particle density of states, since the electron correlation in atoms with partly filled 3d shells is large. The electrostatic interaction between the 2p and 3d electrons results in a localization of the 3d wavefunction in the final state. In calculating the dipole transition from a $3d^n$

0953-8984/92/164189+16$04.50

ground state to the $2p^53d^{n+1}$ final states we have to take into account the 2p–3d and 3d–3d Coulomb and exchange interactions, the 2p and 3d spin–orbit interactions, and the crystal field acting on the 3d states. Calculations for the octahedral crystal field have been performed by Yamaguchi *et al* [3] van der Laan *et al* [4] and de Groot *et al* [5]†, neglecting the 3d spin–orbit interaction. However, this spin–orbit interaction has an important influence on the spectrum, especially on the branching ratio between the $2p_{3/2}$ and $2p_{1/2}$ peaks. In the isotropic absorption spectrum [6] as well as in the magnetic circular dichroism (MXD) (right- minus left-circularly-polarized absorption) [7] the deviation of this branching ratio from the statistical value is proportional to the 3d spin–orbit interaction per hole. Calculations in the presence of the 3d spin–orbit interaction have recently been presented for magnetic circular dichroism [8], but the dependence on the crystal field was not treated in detail.

In order to facilitate the use of $L_{2,3}$ absorption spectroscopy, the current paper provides a systematic study of the 2p→3d excitation spectra for most of the 3d transition metal ions in tetrahedral and octahedral crystal fields with spin–orbit interaction. The method of calculation is described in section 2, and the results are given in section 3. The spectral features are discussed in section 4. The effects of the crystal field are treated in section 5. The interpretation of the spectrum for d^0, the simplest case, is given in section 6. A discussion and conclusions are given in section 7.

2. Theory and calculational method

A 2p electron has dipole-allowed transitions to s- and d-like final states. Due to the large wavefunction overlap, the 3d channel is much stronger than the other channels, and the 2p absorption is determined by the transition probability $3d^n \rightarrow 2p^53d^{n+1}$.

The initial state $3d^n$ of the free ion in spherical symmetry (O_3) is split into levels LSJ by the Coulomb interactions $F^{2,4}$ (d, d) and the spin–orbit interaction ζ(3d). The *ab initio* values of these interactions are given in table 1. When a crystal field reduces the symmetry O_3 to a lower symmetry, the irreducible representations $LSJ$are projected onto representations $\Gamma S\Gamma_J$ of the lower group, where Γ, S and Γ_J are the orbital momentum, spin momentum and total symmetry, respectively. The level with the lowest energy is the ground state. This level, whose representation is given in table 2, is fully occupied at $T = 0$ K. At finite temperatures higher spin–orbit split levels are also partly occupied, but this effect is small if the thermal energy kT (26 meV at room temperature) is smaller than the 3d spin–orbit interaction (table 1).

The final state configuration $2p^53d^{n+1}$ is split by spin–orbit and electrostatic interactions into representations $L'S'J'$ or $\Gamma S'\Gamma'_J$. The *ab initio* values of the involved parameters, $F^{2,4}$(d,d), ζ(2p), ζ(3d), F^2(p,d) and $G^{1,3}$(p,d), are given in table 3. In the actual calculation the Slater integrals of the initial and final state have been scaled down to 80% of the atomic values to account for intra-atomic relaxation effects. In principle these can be included by configuration interaction with the low-energy excited configurations, e.g. in a multiconfigurational Dirac–Fock calculation. However, such an approach has little practical advantage in a solid, since there are a large number of small admixtures to the dominant configuration, and a similar result can be obtained by using reduced Slater integrals for a single configuration [9]. Although

† Their spectra for d^1, d^2, d^3, d^5, d^7 in the atomic case with zero crystal-field contain errors which make them look different from the spectra with a small crystal field.

Table 1. The *ab initio* Hartree–Fock values (eV) of the parameters in the initial-state configurations. The actual values for the Coulomb and exchange interaction used in the calculation have been scaled to 80% of these values.

Configuration	$F^2(d,d)$	$F^4(d,d)$	$\zeta(3d)$
$Ti^3 + d^1$	—	—	0.019
$V^4 + d^1$	—	—	0.031
$V^3 + d^2$	10.128	6.353	0.027
$Cr^3 + d^3$	10.777	6.754	0.035
$Cr^2 + d^4$	9.649	6.000	0.030
$Mn^4 + d^3$	12.416	7.819	0.052
$Mn^3 + d^4$	11.415	7.146	0.046
$Mn^2 + d^5$	10.316	6.412	0.040
$Fe^3 + d^5$	12.043	7.533	0.059
$Fe^2 + d^6$	10.966	6.813	0.052
$Co^3 + d^6$	12.663	7.917	0.074
$Co^2 + d^7$	11.605	7.207	0.066
$Ni^3 + d^7$	13.277	8.294	0.091
$Ni^2 + d^8$	12.234	7.597	0.083
$Cu^2 + d^9$	—	—	0.102

Table 2. The character of the ground state for the high-spin d^n configurations in spherical (O_3), tetrahedral (T_d), and octahedral (O_h) symmetry.

Config.	O_3	T_d	O_h
d^0	$^1S_0$	$(^1A_1)A_1$	$(^1A_1)A_1$
d^1	$^2D_{3/2}$	$(e, {}^2E_2)U'$	$(t_2, {}^2T_2)U'$
d^2	$^3F_2$	$(e^2, {}^3A_2)T_2$	$(t_2^2, {}^3T_1)E$
d^3	$^4F_{3/2}$	$(e^2t_2, {}^4T_1)U'$	$(t_2^3, {}^4A_2)U'$
d^4	$^5D_0$	$(e^2t_2^2, {}^5T_2)A_1$	$(t_2^3e, {}^5E)A_1$
d^5	$^6S_{5/2}$	$(e^2t_2^3, {}^6A_1)U', E'$	$(t_2^3e^2, {}^6A_1)U', E'$
d^6	$^5D_4$	$(e^3t_2^3, {}^5E)A_1$	$(t_2^4e^2, {}^5T_2)T_2$
d^7	$^4F_{9/2}$	$(e^4t_2^3, {}^4A_2)U'$	$(t_2^5e^2, {}^4T_1)E'$
d^8	$^3F_4$	$(e^4t_2^4, {}^3T_1)A_1$	$(t_2^6e^2, {}^3A_2)T_2$
d^9	$^2D_{5/2}$	$(e^4t_2^5, {}^2T_2)E''$	$(t_2^6e^3, {}^2E)U'$

the actual value of the reduction factor κ depends on the specific type of compound, there is a certain consensus to use a value between 0.75 and 0.8 [9]. The smaller value of κ results in a reduced multiplet width and a slightly different $L_{2,3}$ branching ratio [6]. Note that, apart from the crystal field parameter, the only free parameter which appears in the calculation is κ.

The dipole transition probability was obtained with Thole's method [10]. This approach starts with the calculation of the reduced matrix elements of the necessary operators in the spherical group using Cowan's atomic multiplet program [11]. The Wigner–Eckart theorem is then applied to obtain the reduced matrix elements in the desired point group, where the required isoscalar factors are obtained from Butler's point-group program [12].

3. Results

Figures 1–15 show the calculated spectra of the various 3d transition metal ions in

Table 3. The *ab initio* Hartree–Fock values (eV) of the parameters in the final-state configurations. The actual values for the Coulomb and exchange interaction used in the calculation have been scaled to 80% of these values.

Configuration	E(aV)	F^2(d,d)	F^4(d,d)	ζ(2p)	ζ(3d)	F^2(p,d)	G^1(p,d)	G^3(p,d)
$Ti^4+p^5d^1$	464.844	—	—	3.776	0.032	6.302	4.628	2.633
$Ti^3+p^5d^2$	461.222	10.343	6.499	3.776	0.027	5.581	3.991	2.268
$V^4+p^5d^2$	523.326	11.965	7.554	4.650	0.042	6.758	5.014	2.853
$V^3+p^5d^3$	519.943	10.974	6.888	4.649	0.036	6.057	4.392	2.496
$Cr^3+p^5d^4$	581.794	11.595	7.269	5.667	0.047	6.525	4.788	2.722
$Cr^2+p^5d^5$	579.316	10.522	6.550	5.668	0.041	5.840	4.204	2.388
$Mn^4+p^5d^4$	650.186	13.177	8.300	6.845	0.066	7.658	5.776	3.288
$Mn^3+p^5d^5$	646.997	12.210	7.648	6.845	0.059	6.988	5.179	2.945
$Mn^2+p^5d^6$	644.616	11.155	6.941	6.846	0.053	6.321	4.606	2.618
$Fe^3+p^5d^6$	715.556	12.818	8.022	8.199	0.074	7.446	5.566	3.166
$Fe^2+p^5d^7$	713.118	11.779	7.326	8.200	0.067	6.793	5.004	2.844
$Co^3+p^5d^7$	787.306	13.422	8.393	9.746	0.092	7.899	5.951	3.386
$Co^2+p^5d^8$	785.048	12.396	7.706	9.748	0.083	7.259	5.397	3.069
$Ni^3+p^5d^8$	862.229	14.022	8.761	11.506	0.112	8.349	6.332	3.603
$Ni^2+p^5d^9$	860.140	—	—	11.507	0.102	7.721	5.787	3.291
$Cu^2+p^5d^{10}$	938.494	—	—	13.498	—	—	—	—

tetrahedral (T_d) and octahedral (O_h) symmetry. The Cu d^9 spectra have not been given, since they consist only of two lines. The spectra within each panel represent different crystal field strengths 10 Dq, ranging from 0 to 3 eV in increments of 0.5 eV. Obviously, the spectra for 10 $Dq = 0$, corresponding to spherical symmetry, are identical for T_d and O_h. The spectra for the different configurations of each element have been plotted on the same energy scale in order to facilitate comparison. The total intensity of the spectra has been normalized to one. The absolute intensity is $(10 - n)/5$ times larger, thus proportional to the number of holes $(10 - n)$ in the initial state d^n [13]. The calculated line spectra were convoluted with a Lorentzian line shape equal to the lifetime width Γ of the L_3 core hole, [14] and with a Gaussian line width σ to represent instrumental broadening. For the latter we used the source-size-limited resolution of the soft x-ray monochromator on the undulator beamline 5U.1 at the synchrotron radiation facility in Daresbury (UK) [15]. These values are given in table 4. Whilst it is possible to obtain a higher resolution at the expense of intensity, we chose a moderate energy resolution for the following reasons: (i) the majority of users will not have access to ultra-high resolution devices; (ii) a moderate resolution is sufficient to distinguish the differences due to valency and symmetry; (iii) there can be additional broadening of the core hole line width due to e.g. solid state effects.

4. Spectral trends

The 2p spectra consist of a $2p_{3/2}$ (L_3) and $2p_{1/2}$ (L_2) structure with an energy separation (1.5 ζ_p) increasing from 5.7 eV in Ti to 17.3 eV in Ni. This is larger than the increase in the electrostatic interactions F^k and G^k, which is around 30% (table 3). The L_3 and L_2 structures are better separated when the ratio $\zeta(2p)/G^1(2p,3d)$ is larger. This ratio varies from 0.6 to 1.5 across the series, and the heavier elements show a very distinct separation into two structures.

Table 4. The half-width Γ (meV) of the Lorentzian line shape for the L_3 core hole life time broadening [13], and the standard deviation σ (meV) of the source-size-limited resolution of the undulator beamline 5U.1 at the synchrotron facility in Daresbury [14].

Element	Γ	σ
Ti	110	95
V	120	130
Cr	135	151
Mn	160	181
Fe	180	211
Co	215	243
Ni	240	279

The initial state spin–orbit interaction has a large influence on the branching ratio. It splits the degenerate representation ΓS into Γ_J levels, where the branching ratio of the ground state $\Gamma S \Gamma_J$ level is higher than that of the LS average [6]. The spin–orbit interaction can be quenched, which means that the first-order spin–orbit splitting is zero. This occurs for the orbital representations A and E, but not for T_1 or T_2. Second-order spin–orbit splitting mixes the $\Gamma S \Gamma_J$ levels with a mixing coefficient proportional to $\zeta_{3d}/\Delta E$.

Although elements with the same initial state d^n have different Slater integrals in the order of 10% their spectra are nevertheless similar, as is clear from the figures. However, the spectra of different d^n configurations are quite different and this can be used to identify the valency of an element. The energy separation between two oxidation states d^n and d^{n+1} of a particular element is equal to $Q - U$, where Q and U are the 2p–3d and 3d–3d Coulomb interactions, respectively. Since Q is larger than U, the highest oxidation state (d^n) has the highest energy. The difference in average energy between two adjacent oxidation states can also be obtained from table 3, which gives a value between 2 to 4 eV.

5. Effect of the crystal field

The crystal field interaction mixes states with different L values in the ground state LS term, allowing transitions to other final states with the same spin. This gives rise to a broadening of the peaks and a gradual appearance of new peaks with increasing crystal field interaction.

The effect of a small crystal field on the spectral shape is given by the splitting lemma [6]: when there is an interaction which lowers the symmetry of the Hamiltonian, and when only one sublevel of the original ground state is populated, the isotropic dipole spectrum does not change when the splittings in the final state cannot be resolved. Thus, the spectrum shows no abrupt change between spherical symmetry ($10\ Dq = 0$) and a small distortion of say 0.1 eV, even though the ground state representation is changed. The gradual change of the spectra is clearly visible in all panels of figures 1–15. When the symmetry is further reduced from cubic symmetry O_h or T_d to a lower symmetry D_4, D_3, D_2, C_4, C_3 or C_2, the spectral changes are on an energy scale equal to the magnitude of the non-cubic crystal field distortion. Note that the splittings lemma does not apply for the 3d spin–orbit interaction, and that the spectra with and without this interaction are distinctly different.

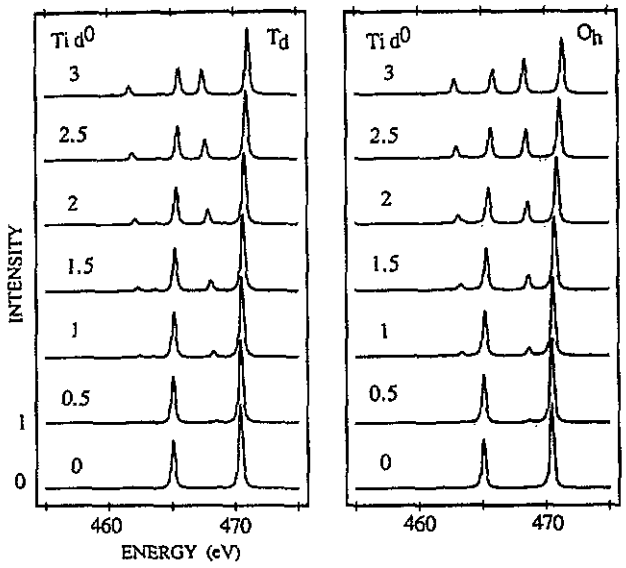

Figure 1. Calculated 2p absorption spectra of *3d transition metal ions in tetrahedral* (T_d) and octahedral (O_h) symmetry. The Slater integrals and spin–orbit parameters are 80% and 100% of the atomic values, respectively. The values of the convolution are given in table 4. The numbers near the spectra indicate the values of 10 Dq. The spectra have a total intensity equal to one and have been shifted vertically for clarity.

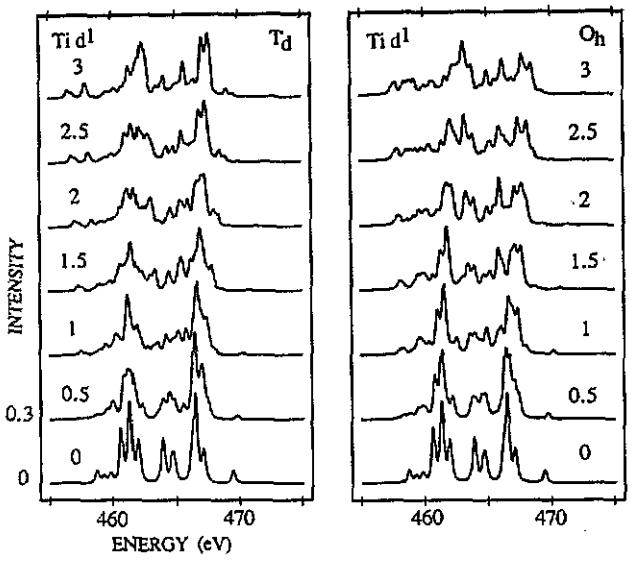

Figure 2. Ti d^1.

Abrupt changes in the spectra are indicative of spin transitions. For a small crystal field the configuration has high spin, but when the crystal field exceeds the energy gain of the spin pairing, the spin state changes to low spin (or intermediate spin). These transitions are possible in d^3 to d^7 for a value of 10 Dq between 1.5 and

3.5 eV as given in table 5. (In figures 1–15 the crystal field has been limited to 3 eV, because higher values are relatively less common.) The spectra of the low-spin states have a higher average energy and a lower branching ratio than those of the high-spin states. The branching ratios in O_h symmetry can be found in [8]. An example of a spin transition is seen for Cr or Mn d^4 in T_d between 10 Dq 1.5 and 2 eV, where the high-spin $e^2t_2^2$ ($S = 2$) configuration changes into low-spin e^3t_2 ($S = 1$) while the branching ratio reduces from 0.72 to 0.58.

Table 5. The values of 10 Dq (eV) where the high-spin state has changed to low-spin.

Configuration	T_d	O_h
Cr d^3	2.5	—
Mn d^3	3	—
Cr d^4	2	2.5
Mn d^4	2	3
Mn d^5	3	3
Fe d^5	3.5	3.5
Fe d^6	3	2
Co d^6	3.5	2.5
Co d^7	—	2.5
Ni d^7	—	3

Globally, the spectra in figures 1–15 consist of two structures moving apart with 10 Dq. When either the e or t_2 level in the ground state is full, only one structure remains in the $2p_{3/2}$ and $2p_{1/2}$ multiplets are less wide. This can be verified for the following configurations in T_d: e^4 (low-spin), d^6 ($e^4t_2^2$), d^7($e^4t_2^3$), d^8 ($e^4t_2^4$), and d^9 ($e^4t_2^5$); and in O_h: t_2^6 (low-spin), d^8 ($t_2^6e^2$), and d^9 ($t_2^6e^3$).

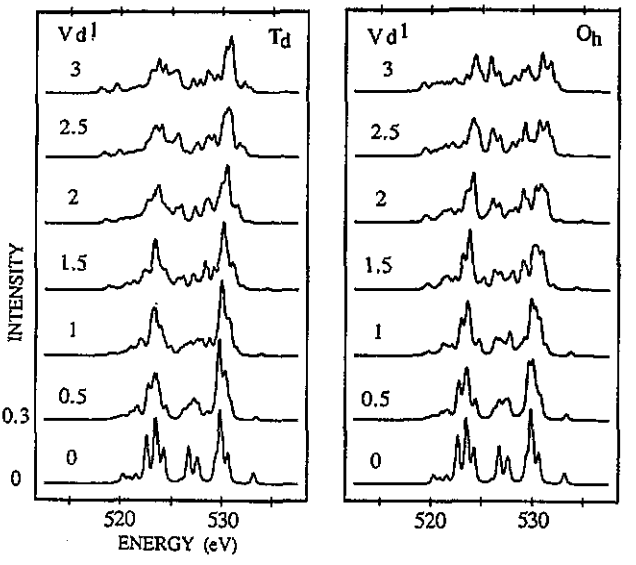

Figure 3. V d^1.

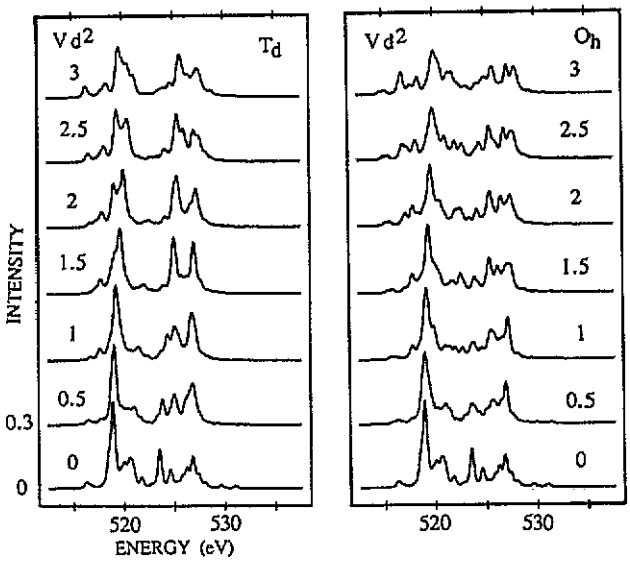

Figure 4. V d^2.

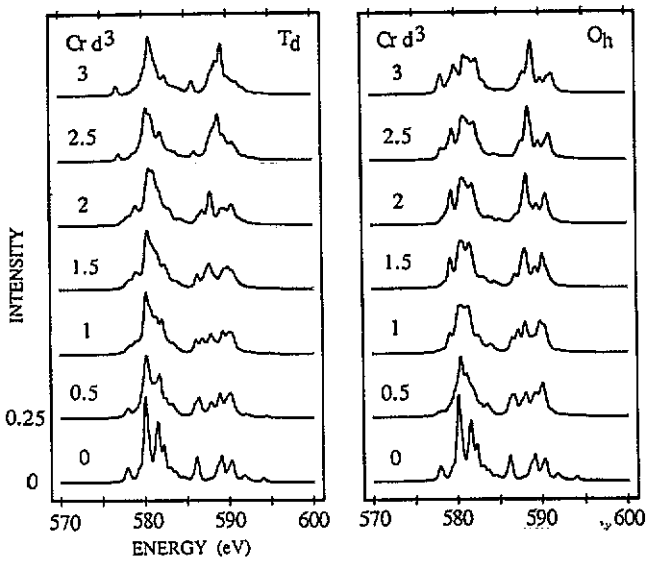

Figure 5. Cr d^3.

6. d^0 spectrum

In general there are too many individual dipole transitions to allow a simple interpretation of the spectra. An additional complication is the use of intermediate coupling, since neither jj nor LS are good approximations for the exact momentum coupling. The only simple transition is $d^0 \rightarrow p^5d^1$, where the initial state has neither electrostatic nor spin–orbit interaction. From the initial state configuration $d^0\,{}^1S$, only final states can be reached which have the representation ^1P of the polarization vector

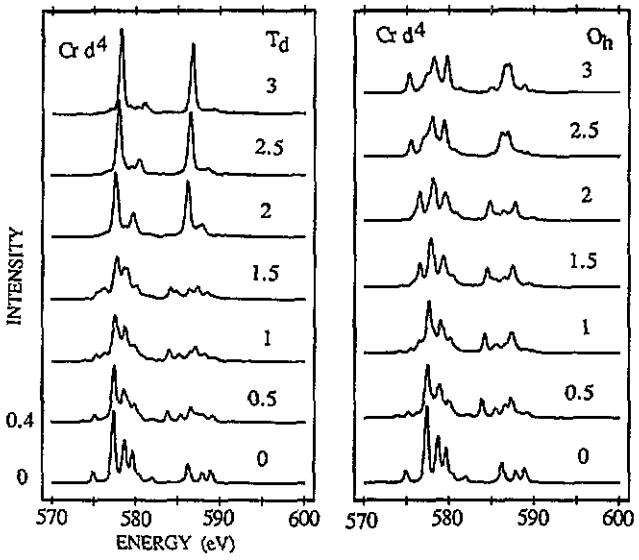

Figure 6. Cr d^4.

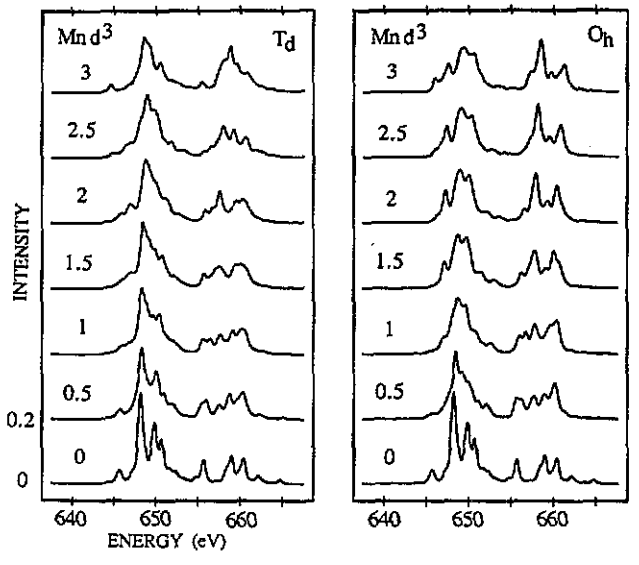

Figure 7. Mn d^3.

of the x-rays. Of the final state terms ^3F, ^3D, ^3P, ^1D and ^1P, only the last one is therefore accessible. Thus, without spin–orbit interaction there is only one line. In the presence of spin–orbit interaction the total angular momentum selection rule is $\Delta J = J' - J = \pm 1$, $0 (J = J' = 0$ excluded). Transitions are now allowed to the three final-state levels $J' = 1$, which are mixtures of the $^1P_1$, $^3D_1$ and $^3P_1$ levels. In jj coupling, which holds when there are no electrostatic interactions, the three allowed final state $J' = 1$ levels are $p_{3/2}d_{3/2}$, $p_{3/2}d_{5/2}$ and $p_{1/2}d_{3/2}$, with an intensity

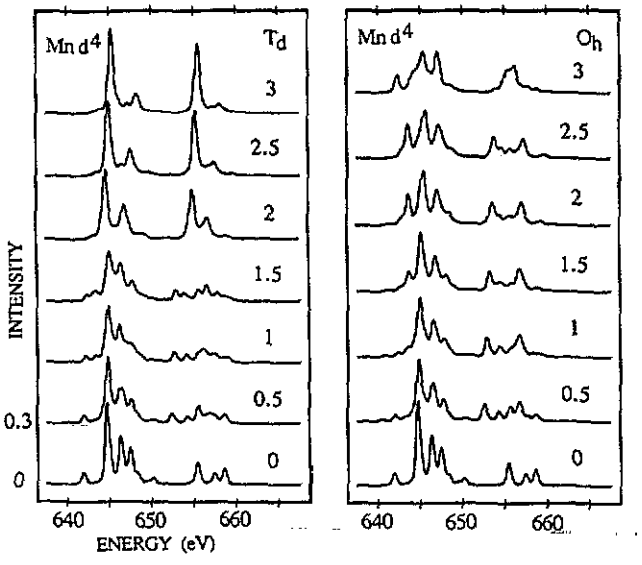

Figure 8. Mn d^4.

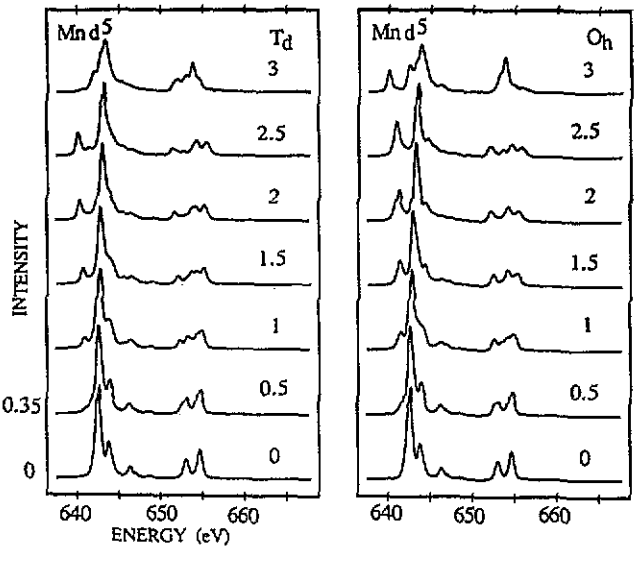

Figure 9. Mn d^5.

ratio of 2:8:5. With p–d interaction the branching ratio B, which is defined as the intensity ratio $p_{3/2}/(p_{3/2} + p_{1/2})$, changes from the statistical value 2/3 to a lower value. The reason for this is that with increasing $U(p,d)/\zeta(2p)$, the distribution of the spin character changes smoothly to the pure LS coupled case with $\zeta(2p) \rightarrow 0$, where only the transition to the ^1P state is allowed [6].

In a cubic field the initial state has the representation $^1A_1$, and only final states can be reached which have the representation $^1T_1$ of the x-ray polarization vector.

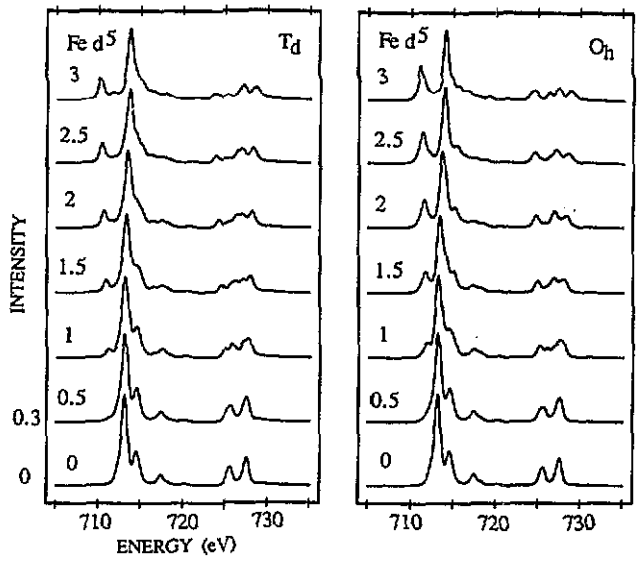

Figure 10. Fe d^5.

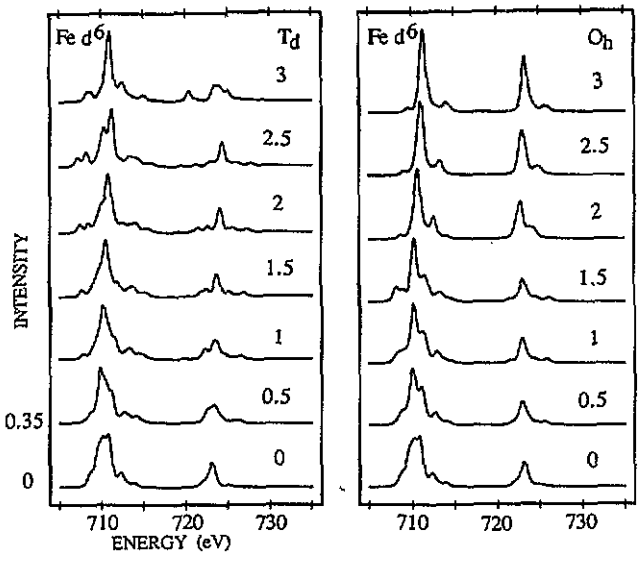

Figure 11. Fe d^6.

The final-state configuration spans A_1 (2×), A_2 (3×), E (5×), T_1 (7×) and T_2 (8×) as irreducible representations. The seven T_1 levels in O_h correspond to the $J' = 1$ (3×), $J' = 3$ (3×) and $J' = 4$ levels in O_3. The $d_{3/2}$ branches to U′ and the $d_{5/2}$ to U′ + E″, while the $p_{1/2}$ and $p_{3/2}$ branch to E′ and U′, respectively. The product of the representations for p and d must contain the dipole operator T_1, which is fulfilled for all transitions except E″ → E′. Thus, the final states with total symmetry T_1 are $p_{3/2}(U')d_{3/2}(U')[J' = 1,3]$, $p_{3/2}(U')d_{3/2}(E'',U')[J' = 1,3,4]$,

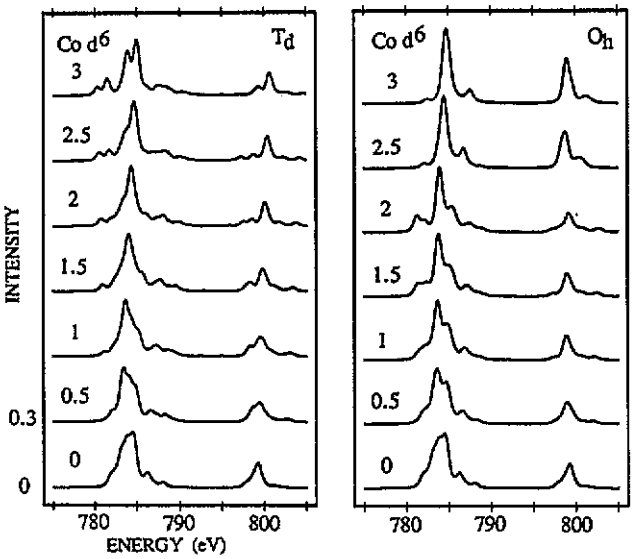

Figure 12. Co d^6.

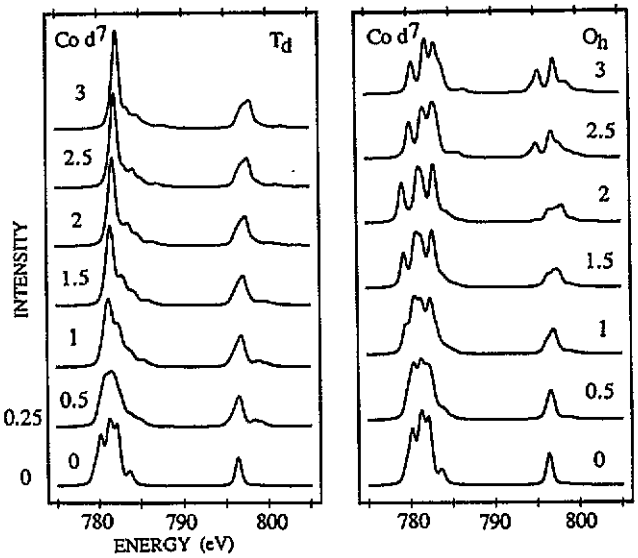

Figure 13. Co d^7.

$p_{1/2}(E')d_{3/2}(U')[J' = 1]$ and $p_{1/2}(E')d_{5/2}(U')[J' = 3]$. There are therefore two levels in the L_2, and five in the L_3 edge. The $d(E'')$ level has pure t_2 character and the two $d(U'')$ levels have t_2 and e character mixed by first-order spin–orbit interaction. For small 10 Dq the T_1 levels which branch from $J' = 3$ and 4 have a low intensity, and only the three $J' = 1$ levels of mixed t_2 and e character remain. For large 10 Dq the core–hole interaction becomes less important, and the seven levels are grouped into four separate lines, viz. $p_{1/2}d(t_2)$, $p_{1/2}d(e)$, $p_{3/2}d(t_2)$ (3×),

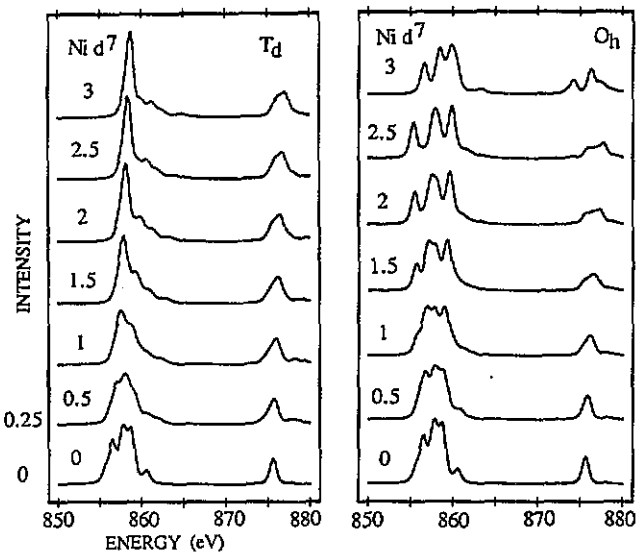

Figure 14. Ni d^7.

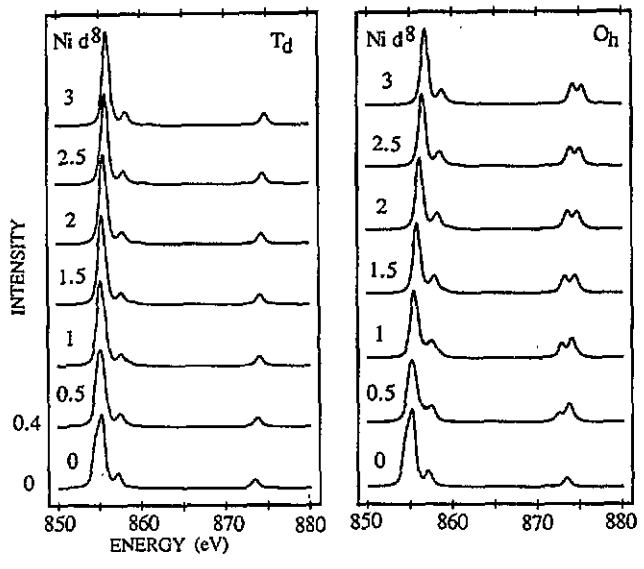

Figure 15. Ni d^8.

$p_{3/2}d(e)$ (2×). The e and t_2 states will have an intensity ratio of 4:6 and an energy separation of 10 Dq.

The spectra of $d^n(n \neq 0)$ can be analysed in a similar manner. However, the ground state J is then not equal to zero. There are final states of e.g. $J' = 2$ which split into e and t_2, and a single peak splits into two peaks with a separation proportional to the field. This does not happen in the d^0 spectrum, where $J' = 1$ does not split but goes to a representation t_1, so only forbidden lines can gain

intensity.

7. Discussion and conclusion

We have presented the $L_{2,3}$ spectra of 3d transition metal ions in cubic symmetry. Lower symmetries will give similar spectra when the non-cubic distortion is small. To demonstrate the usefulness of the local approach we give an example for the Fe 2p absorption spectrum of α-Fe_2O_3 (hematite), which has a rhombohedral chromium sesquioxide structure (space group D^6_{3d}). In the trigonal distorted octahedral symmetry the iron is surrounded by six oxygen atoms at distances 1.91 and 2.06 Å. Figure 16 shows the experimental spectrum (*a*) [16], together with the calculated spectrum (*b*) for Fe d^5 with $\kappa = 0.75$, 10 Dq (O_h) = 1.8 eV convoluted by $\Gamma = 0.18$ and $\sigma = 0.5$ eV. For comparison spectrum (*c*) gives the calculation with 10 Dq (O_h) = 1.5 eV from figure 10. It is clear that all structure is extremely well reproduced, even the small peaks at the high-energy side of the L_3 edge. The slight asymmetry in the experimental spectrum is due to solid state effects, which are not included in the single configuration calculation. The intensity of the leading peak in the L_3 as well as L_2 edge is too low in the calculation. This can be improved by including the crystal field parameters for the trigonal distortion. Other comparisons between experiment and theory have been reported for Mn impurity in metals [17], titanium oxides [18], nickel oxide and dihalides [19], high- and low-spin divalent nickel compounds [4], iron phthalocyanine [20] and 3d transition metal containing minerals [16]. Good agreement between calculated and experimental results was found in all cases of strongly electronegative anions (F, Cl, O); however, the agreement was worse for more covalent compounds.

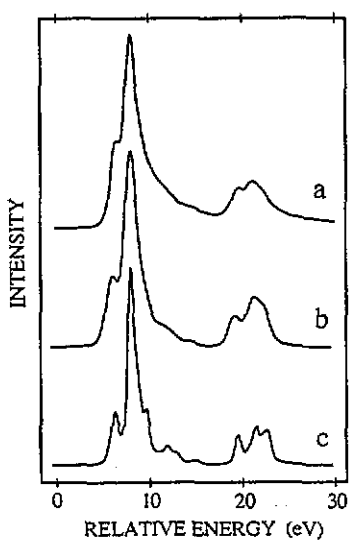

Figure 16. The experimental Fe 2p XAS spectrum of (*a*) Fe_2O_3; (*b*) the calculated Fe d^5 spectrum with $\kappa = 0.75$, 10 Dq (O_h)=1.8 eV, convoluted by $\Gamma = 0.18$ and $\sigma = 0.5$ eV; (*c*) and the calculated spectrum with 10 Dq (O_h)=1.5 eV from figure 10.

The reason for the good agreement between ionic compounds can be understood as follows: these compounds obtain their stability primarily from the Madelung energy, which is the energy gain obtained by the transfer of electrons from the cation to anion sites. This results in an integer number of d electrons, so that the absorption process can be described by a transition $3d^n \rightarrow 2p^5 3d^{n+1}$. The presence of s character in the valence band does not affect the spectral shape, because: (i) the transition probability to the s states is small; and (ii) the s–d interaction can be neglected compared to the d–d and p–d interactions.

For less electronegative anions in more covalent compounds, the Madelung term is less important and the d-count can reach a non-integer value. The ground state of these covalent materials is a mixture of configurations $3d^n$, $3d^{n+1}\underline{L}$, $3d^{n+2}\underline{L}^2$, etc. where $\underline{L}$ denotes a ligand hole [19, 21]. The final state is a mixture of configurations $2p^5 3d^{n+1}$, $2p^5 3d^{n+2}\underline{L}$, etc. If the energy difference between two adjacent configurations in the initial state is equal to ΔE, then the energy difference between the accessible final-state configurations is equal to $\Delta E' = \Delta E - Q + U$. The value of $Q - U$ is of the order of a few eV (as described in section 4). When ΔE is large compared with $Q - U$, the influence of the configuration interaction is small and the spectrum is that of a single configuration. However, when the energy difference between the configurations is small and there is a large hybridization (mixing), the final-state levels with the same representation have interference. This can result in the deformation of the multiplet structures and the appearance of satellite structures (cf shake-up in photoemission). This effect has been found for the more covalent ligands of the Ni dihalides series [19] and is also observed in sulphides, antimonides, cyanides, and phthalocyanines [22]. Thus for covalent compounds the calculated spectra for single configurations should serve only as a starting point for a more complete analysis taking into account the mixing between the configurations.

Summarizing, the calculated spectra can be used to obtain the valency and the crystal field parameters from the experimental $L_{2,3}$ spectra for ionic compounds. For covalent materials a proper analysis should also take the mixing between the different configurations into account.

References

[1] Chen C T and Sette F 1989 *Rev. Sci. Instrum.* **60** 1616
[2] Chen C T and Sette F 1990 *Phys. Scr.* T **31** 119
[3] Yamaguchi T, Shibuya S, Suga S and Shin S 1982 *J. Phys. C: Solid State Phys.* **15** 2641
[4] van der Laan G, Thole B T, Sawatzky G A and Verdaguer M 1988 *Phys. Rev.* B **37** 6587
[5] de Groot F M F, Fuggle J C, Thole B T and Sawatzky G A 1990 *Phys. Rev.* B **42** 5459
[6] Thole B T and van der Laan G 1988 *Phys. Rev.* B **38** 3158
[7] van der Laan G and Thole B T 1990 *Phys. Rev.* B **42** 6670
[8] van der Laan G and Thole B T 1991 *Phys. Rev.* B **43** 13401
[9] Lynch D W and Cowan R D 1987 *Phys. Rev.* B **36** 9228
[10] Thole B T unpublished
[11] Cowan R D 1981 *The Theory of Atomic Structure and Spectra* (Berkeley: University of California Press)
[12] Butler P H 1981 *Point Group Symmetry, Applications, Methods and Tables* (New York: Plenum)
[13] Thole B T and van der Laan G 1988 *Phys. Rev.* A **38** 1943
[14] Krause M O and Oliver J H 1979 *J. Phys. Chem. Ref. Data* **8** 329
[15] Mythen C S, van der Laan G and Padmore H A 1992 *Rev. Sci. Instrum.* **63** 1313
[16] Cressey G, Henderson C M B and van der Laan G unpublished
[17] Thole B T, Cowan R D, Sawatzky G A, Fink J and Fuggle J C 1985 *Phys. Rev.* B **31** 6856

[18] van der Laan G 1990 *Phys. Rev.* B **41** 12366
[19] van der Laan G, Zaanen J, Sawatzky G A, Karnatak R C and Esteva J M 1986 *Phys. Rev.* B **33** 4253
[20] Thole B T, van der Laan G and Butler P H 1988 *Chem. Phys. Lett.* **149** 295
[21] van der Laan G, Westra C, Haas C and Sawatzky G A 1981 *Phys. Rev.* B **23** 4369
[22] Thole B T, van der Laan G *et al* unpublished